Theoretical Study of Intramolecular Long-Range Electron Transfer Reactions between Porphyrin and Benzoquinone: Ab Initio Calculations of Electronic Coupling Element

Shigehiko Hayashi[†] **and Shigeki Kato***

Department of Chemistry, Graduate School of Science, Kyoto University, Kitashirakawa, Sakyo-ku, Kyoto 606, Japan

Received: June 17, 1997; In Final Form: November 24, 1997

The electronic coupling elements (ECEs) in the long-range intramolecular electron transfer systems with porphyrin−benzoquinone donor/acceptor groups linked by organic spacers are investigated theoretically. A method for calculating the electronic coupling element is developed based on ab initio molecular orbital theory. The ECEs are expressed in terms of the Hamiltonian matrix elements of singly excited configuration interaction wave functions with the localized donor, acceptor, and spacer orbitals. Compared to the hole transfer mechanism, the electron transfer through the unoccupied spacer orbitals is found to be the responsible mechanism in the present systems. The ECEs are examined by the decomposition and pathway analysis methods. The results were that (a) the ECEs strongly depend on the geometries of spacer molecules, (b) the through bond type interaction involving the π^* orbitals of benzene parts in the spacers gives significant contributions to the ECEs, and (c) the interference between the electron pathways plays an important role in determining the ECEs.

1. Introduction

Long-range electron transfer from electron donor to acceptor sites linked by organic spacers has received much attention both from experimental and theoretical points of view in recent years because of their importance in chemical and biological systems.[1] Experimentally, spacer species have been introduced to biphenyl−naphthyl decalines,[2−7] dimethoxynaphthalene−dicyanoethylene,[8,9] and porphyrin−quinone[1,10,11] pairs in order to investigate the effects of donor−acceptor distance and mutual orientation on the electron transfer rates. The importance of characters of spacer chemical bonds has been also recognized in determining the rate constants, because the indirect through-bond[12,13] type electronic coupling between the donor and acceptor is responsible to these long-range electron transfer reactions. Among various types of donor−acceptor pairs, the photoinduced electron transfer processes in porphyrin−quinone pairs[1,10,11] have been extensively studied since these systems are regarded as model compounds for the photosynthetic systems in nature.

It is known that the reaction rate of long-range electron transfer, k_{LRET}, is given by Fermi's golden rule with the Condon approximation,[14]

$$k_{\mathrm{LRET}} = \frac{2\pi}{\hbar}|V_{RP}|^2\langle\{\mathrm{FCWD}\}\rangle_{\mathrm{R}} \qquad (1)$$

where V_{RP} is the electronic coupling element (ECE) between the reactant and product states and $\langle\{\mathrm{FCWD}\}\rangle_{\mathrm{R}}$ is the Franck−Condon weighted density of states, respectively. Theoretical studies[15−37] have been carried out to understand the role of spacers in determining the magnitude of the ECE. These studies have revealed that the dominant contribution to long-range ECE comes from the indirect electron coupling attributed to the through-bond interaction in the spacers.

In order to elucidate the mechanism of indirect coupling, several methods for the pathway analysis[20−37] have been proposed and applied to chemical and biological systems using ab initio and semiempirical molecular orbital (MO) methods. In these analyses, the ECE is expressed as the sum of contributions from the pathways starting from the donor orbitals and reaching the acceptor ones through the spacer atoms or bonds. It has been found that the ECE is mainly determined by several dominant pathways and the interference among them reflecting the structure of spacer plays an important role to determine the magnitude of total ECE. In spite of the activities of these theoretical studies on the ECE in long-range electron transfer, many studies have concerned the spacers including saturated hydrocarbon bonds and modeled the donor and acceptor moieties with replacing by simple groups such as CH_2.

In the present study, we performed ab initio MO calculations for the photoinduced electron transfer of the porphyrin−quinone systems, **1** and **2**, shown in Figure 1. Recently, Sakata et al. have studied the reaction processes of such compounds in polar solvents experimentally.[38] They found that reaction rates for the compounds including bicyclo ring as the spacer are much faster (∼30 times) than that of **1**, indicating that the bicyclo ring is responsible for such enhancement of the electron transfer rates. We calculated here the ECEs between the porphyrin and quinone to elucidate the origin of such difference of the rates. Since the reactions take place in the electronically excited states, we employed singly excited configuration interaction (SECI) wave functions to estimate the ECEs as well as to define the reactant, product, and intermediate electronic states. We devised a method to define the localized orbitals by the unitary transformations of canonical MOs of the whole reaction systems in constructing the SECI wave functions.

The purpose of present study is 2-fold. One is to clarify the role of spacers in the photoinduced electron transfer processes of the present molecular systems based on the pathway analyses. In particular, we focus on the difference of contributions from

[†] Research Fellow of the Japan Society for the Promotion of Science.

S1089-5639(97)01978-6 CCC: $15.00
Published on Web 04/04/1998

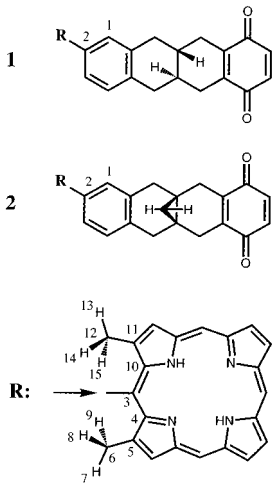

Figure 1. Structures of porphyrin−quinone photoinduced electron transfer systems, **1** and **2**. The arrow indicates the porporphyrin carbon atom to which the spacer is attached.

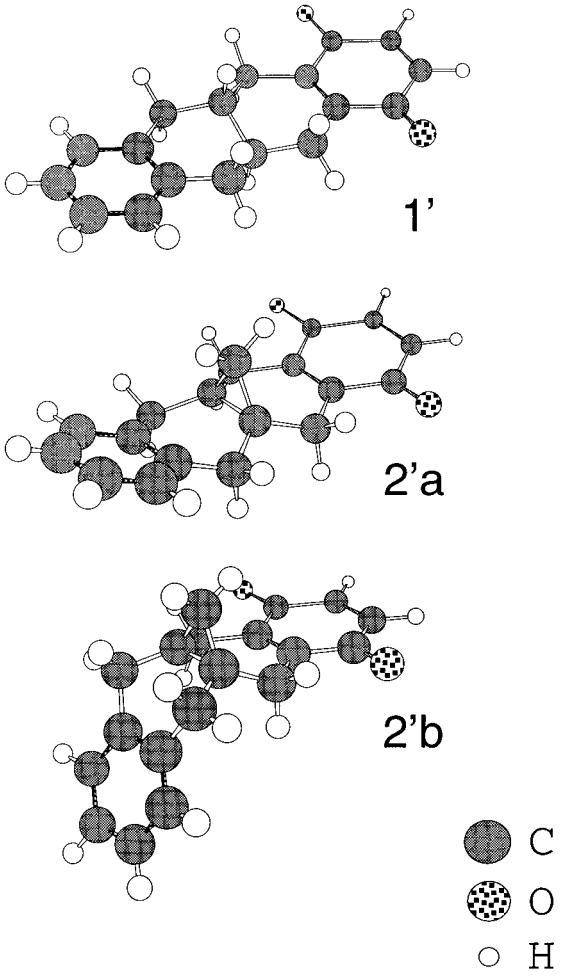

Figure 2. Geometries of the subsystems, **1′**, **2′a**, and **2′b**.

π and σ orbitals in determining the magnitudes of ECEs. Another is to construct a realistic molecular model for the photoinduced long-range intramolecular electron transfer reactions with the aid of ab initio MO calculations. We will present the results of molecular dynamics calculations on the mechanism of electron transfer in polar solvents in a future paper.

In the following section, we give details of the geometries of **1** and **2** determined by the present ab initio MO calculations. In section 3, the theoretical models for calculating the ECE employed are presented. Section 4 contains the calculated results of the overall ECEs and the pathway analyses. Conclusions are summarized in section 5.

TABLE 1: Geometric Parameters[a]

C2−C3	1.496
C5−C6, C11−C12	1.524
C6−H7, C6−H8, C6−H9	1.090
C12−H13, C12−H14, C12−H15	1.090
C1−C2−C3 (**1**)	120.1
Cl−C2−C3 (**2a**)	120.0
Cl−C2−C3 (**2b**)	119.9
C2−C3−C4	117.5
C4−C5−C6	125.0
C5−C6−H7, C5−C6−H8, C5−C6−H9	109.5
C10−C11−C12	124.4
C11−C12−H13, C11−C12−H13, C11−C12−H15	109.5
C1−C2−C3−C4	−90.0
C3−C4−C5−C6, C3−C10−C11−C12	0.0
C4−C5−C6−H7, C10−C11−C12−H13	180.0
C4−C5−C6−H8, C10−C11−C12−H15	60.0
C4−C5−C6−H9, C10−C11−C12−H14	−60.0

[a] In angstroms and degrees.

2. Molecular Systems

The molecular systems studied in the present work consist of three parts, dimethylporphyrin as the electron donor, benzoquinone as the acceptor, and the spacers linking with them. For the spacers, we chose two species as shown in Figure 1. We first carried out ab initio calculations to determine the geometries of spacers which are experimentally unknown, because the ECEs for such long-range electron transfer processes strongly depend on the geometries of spacers. Since the geometry optimization calculations for the whole systems including the donor and acceptor are computationally too demanding, we optimized the geometries of the model systems, **1′** and **2′** in Figure 2, which are constructed by replacing the dimethylporphyrin part by the hydrogen atom.

We employed Hartree−Fock (HF) wave functions with the split valence 3-21G basis set. The optimized geometries are shown in Figure 2. For the system involving the bicyclo ring, **2′**, we found two equilibrium geometries, **2′a** and **2′b**. The planes of benzene and quinone parts are almost in parallel with each other in **2′a** as in the case of **1′**, while the molecular plane of **2′b** is strongly bended at the bicyclo ring site. The energy calculated at **2′a** structure was slightly lower (1.1 kcal/mol) than that at **2′b**. In order to see the effect of basis set on the relative stability of these two structures, we repeated the HF calculations with the 6-31G* basis set at the 3-21G-optimized geometries. The resultant energy of **2′a** was slightly higher (3.3 kcal/mol) than the **2′b**. Considering that the difference of energies between **2′a** and **2′b** is small, both the structures may exist in real systems.

For the donor part, we used the geometry of porphyrin obtained by Foresman et al.[39] who carried the HF geometry optimization calculations with the use of 3-21G basis set.

Geometries of the whole donor−acceptor systems, Figure 1, were constructed using the optimized geometries of the subsystems, **1′**, **2′a**, **2′b**, and porphyrin. The geometric parameters required for this purpose are summarized in Table 1. The atomic numbers are defined in Figure 1. The geometry for the dimethyl group and the C2−C3 bond distance were determined on the basis of the experimental values for toluene and biphenyl, respectively. The directions of C2−C3, C5−C6, and C11−C12 bonds were taken to be coincide with those of the corresponding C−H bonds in the subsystems. The dihedral

angles of C1−C2−C3−C4 were assumed to be 90° because these angles are hindered by the steric effect of the dimethyl groups.

We carried out single point HF/3-21G calculations for the whole systems **1**, **2a**, and **2b** at the geometries determined above. The difference in energies between **2a** and **2b** (1.1 kcal/mol) was almost the same as that between their partial systems, **2′a** and **2′b**, indicating that the relative stability between **2a** and **2b** is not altered by the substitutions of dimethylporphyrin groups.

3. Theoretical Methods

3.1. Electronic Coupling Element. Using the perturbation theory,[15,40] the ECE between the reactant (R) and product (P) states is represented by

$$V_{RP} = V_{RP}^{\mathrm{dir}} + V_{RP}^{\mathrm{indir}} \tag{2}$$

where V_{RP}^{dir} is the direct or through space ECE and V_{RP}^{indir} the indirect or through bond one, respectively. The direct term is given by

$$V_{RP}^{\mathrm{dir}} = \langle \phi_R | \hat{H}_{\mathrm{el}} | \phi_P \rangle \tag{3}$$

where $\hat{H}_{\mathrm{el}}$ is the electronic Hamiltonian and $|\phi_R\rangle$ and $|\phi_P\rangle$ are the electronic wave functions of the reactant and product states, respectively. The indirect term comes from the coupling through the intermediate (I) states and is written as

$$V_{RP}^{\mathrm{indir}} = \sum_{i,j} H_{R I_i} G_{ij}(E) H_{I_j P} \tag{4}$$

where H_{KL}, is the Hamiltonian matrix element between the states K and L,

$$H_{\mathrm{KL}} = \langle \phi_{\mathrm{K}} | \hat{H}_{\mathrm{el}} | \phi_{\mathrm{L}} \rangle \tag{5}$$

and the index I_i denotes the intermediate state i. $G_{ij}(E)$ in eq 4 is the matrix element of the Green function for the intermediate states:

$$\hat{G}(E) = \frac{1}{E - \hat{H}_{\mathrm{el}}^{I}} \tag{6}$$

where $\hat{H}_{\mathrm{el}}^{I}$ is the electronic Hamiltonian projected on the space of the intermediate states and E is the tunneling energy, respectively. It is convenient to expand the Green function into a perturbation series:

$$\begin{aligned} G(E) &= \hat{G}^0(E) + \hat{G}^0(E)\hat{V}\hat{G}(E) \\ &= \hat{G}^0(E) + \sum_{n=1}^{\infty} \hat{G}^0(E)(\hat{V}\hat{G}^0(E))^n \end{aligned} \tag{7}$$

where $\hat{G}^0(E)$ is the zeroth order Green function and $\hat{V}$ is the perturbation. If we take the diagonal elements of $\hat{H}_{\mathrm{el}}^{I}$ as the unperturbed Hamiltonian, the matrix elements of the zeroth order Green function are given by

$$G_{ij}^0(E) = \frac{\delta_{ij}}{E - E_i} \tag{8}$$

and those of the full Green function are expressed as[20]

$$\begin{aligned} G_{ij}(E) &= \frac{\delta_{ij}}{E - E_i} + \sum_k \frac{1}{E - E_i} V_{ik} G_{kj}(E) \\ &= \frac{\delta_{ij}}{E - E_i} + \frac{1}{E - E_i} V_{ij} \frac{1}{E - E_j} + \\ &\qquad \sum_k \frac{1}{E - E_i} V_{ik} \frac{1}{E - E_k} V_{kj} \frac{1}{E - E_j} + \ldots \end{aligned} \tag{9}$$

where E_i is the energy of the intermediate state i and V_{ij} is the off-diagonal elements of $\hat{H}_{\mathrm{el}}^{I}$.

We employed SECI wave functions to describe the electronic structures in the electron transfer systems. The Hamiltonian matrix element between the singly excited electronic configurations is given by

$$\langle {}^1\Psi(a \rightarrow r) | \hat{H}_{\mathrm{el}} | {}^1\Psi(b \rightarrow s) \rangle = \epsilon_{rs}\delta_{ab} - \epsilon_{ab}\delta_{rs} - (rs|ba) + 2(ra|bs) + \delta_{ab}\delta_{rs}E_0 \tag{10}$$

where $|{}^1\Psi(a \rightarrow r)\rangle$ is the configuration state function (CSF) generated by the single excitation from the orbital a to the orbital r. E_0 is the energy of the ground state, ϵ_{ij} the Fock matrix element, and δ_{ij} the Kronecker delta, respectively. It is noted that the Fock matrix in eq 10 is not diagonal if the localized MOs (LMOs) which are unitary transformed from the canonical molecular orbitals (CMOs) are used. The off-diagonal elements of the Fock matrix represent the interaction between the LMOs.

The reactant and product electronic states are expressed by the SECI wave functions as

$$|\phi_R\rangle = \sum_{i,j} |{}^1\Psi[\pi_i(\mathrm{Por}) \rightarrow \pi_j^*(\mathrm{Por})]\rangle C^R{}_{ij} \tag{11}$$

$$|\phi_P\rangle = \sum_{i,j} |{}^1\Psi[\pi_i(\mathrm{Por}) \rightarrow \pi_j^*(\mathrm{Qui})]\rangle C_{ij}^P \tag{12}$$

where π_i(Por) and π_i^*(Por) denote the π and π^* orbitals of porphyrin part and π_i^*(Qui) the π^* orbitals of quinone part, respectively. C_{ij}^R and C_{ij}^P are CI coefficients for the R and P. The intermediate electronic states are described by the following configurations:

$$|\phi_{I_i[d \rightarrow s^*]}\rangle = |{}^1\Psi[\pi_d(\mathrm{Por}) \rightarrow \psi_i^*(\mathrm{Sp})]\rangle \tag{13a}$$

$$|\phi_{I_i[s \rightarrow a^*]}\rangle = |{}^1\Psi[\psi_i(\mathrm{Sp}) \rightarrow \pi_{a^*}^*(\mathrm{Qui})]\rangle \tag{13b}$$

$$|\phi_{I_i[s \rightarrow d^*]}\rangle = |{}^1\Psi[\psi_i(\mathrm{Sp}) \rightarrow \pi_{d^*}^*(\mathrm{Por})]\rangle \tag{13c}$$

$$|\phi_{I_{ij}[s \rightarrow s^*]}\rangle = |{}^1\Psi[\psi_i(\mathrm{Sp}) \rightarrow \psi_j^*(\mathrm{Sp})]\rangle \tag{13d}$$

where ψ_i(Sp) and ψ_i^*(Sp) denotes the occupied and unoccupied spacer orbitals. It is noted that the "electron" transfer pathways in the charge separation processes are represented by the configurations in eq 13a. On the other hand, the intermediate states in eqs 13b and 13c contribute to the "hole" transfer pathways. The hybrid "electron/hole" transfer pathways are expressed by the configurations in eq 13d. The characters of these pathways will be discussed in section 4.1.

3.2. Donor, Acceptor, and Spacer Orbitals. We obtained the donor, acceptor, and spacer orbitals to construct the SECI wave functions in eqs 11−13 by the unitary transformations of CMOs of the whole systems. The occupied and unoccupied

TABLE 2: Energies (eV) of π and π^* Orbitals of Donors and Acceptors

	1	2a	2b
π(2nd HOMO; porphyrin)	−6.679	−6.689	−6.682
π(HOMO; porphyrin)	−6.225	−6.235	−6.229
π^*(LUMO; porphyrin)	0.493	0.484	0.491
π^*(2nd LUMO; porphyrin)	0.601	0.590	0.597
π^*(LUMO; quinone)	0.482	0.458	0.470

orbitals were transformed separately. The orbital sets were determined by the procedure including the following three steps: the determination of (1) the donor and acceptor π and π^* orbitals, (2) the spacer π and π^* orbitals, and (3) the valence σ and σ^* orbitals.

3.2.1. Donor and Acceptor π Orbitals. The π and π^* orbitals of donor and acceptor parts were first determined by the corresponding orbital transformation[41] (COT) to the reference donor and acceptor orbitals which were obtained by the calculations of isolated porphyrin and benzoquinone molecules with the 3-21G basis set. The geometries of reference molecules were taken to be equivalent to those of the corresponding parts of the whole systems. The C−C bonds linking to the spacer parts were replaced by the C−H bonds with the length of 1.07 Å in the reference molecules.

We chose 13 π and 11 π^* orbitals of porphyrin and 4 π and 4 π^* orbitals of benzoquinone as the reference orbitals. After the COTs were performed separately both for the donor and acceptor parts, the donor and acceptor orbital sets were symmetric orthogonalized because there were very small overlaps between the donor and acceptor orbitals. We further diagonalized the Fock matrices for the donor and acceptor orbital spaces to obtain the canonical-like π and π^* orbitals localized to the donor and acceptor regions.

The energies of π and π^* orbitals important to describe the *R* and *P* electronic states are tabulated in Table 2. The two highest occupied π and two lowest unoccupied π^* orbitals of porphyrin part constitute the Gouterman's four orbital model.[42] As seen in Table 2, the energies of these orbitals are almost independent of the spacers and the differences are within 0.6 kcal/mol. This indicates that the transferability of donor and acceptor π and π^* orbitals is well achieved in the present procedure and, therefore, it is possible to compare the ECEs between all the systems considered here using the resultant localized donor and acceptor orbitals.

3.2.2. Spacer π Orbitals. In order to accomplish the pathway analyses based on eq 9, it is useful to define LMOs for the spacer because the pathways of electron transfer are well visualized with the use of LMOs. However, the present systems contain benzene rings in the spacers and LMOs are not suitable to represent the π orbitals of benzene part. Therefore we employed the same COT procedure as in section 3.2.1 to determine the π and π^* orbitals of benzene moiety. The reference orbitals were calculated at the same geometry in the spacer with the replacement of the C−C bonds by the C−H ones, and the COTs were carried out separately both for the occupied and unoccupied manifolds. Since there exist degeneracies in these π and π^* orbitals because the geometry is very close to the D_{6h} symmetry even in the spacer and the transformation among the degenerated orbital pair can not be uniquely determined, we further transformed these π and π^* orbitals by diagonalizing the dipole moment matrices. The directions of dipole moment operators were chosen to be along the direction of C_2 axis for **1** spacer and that of the crossing line of the C_s reflection plane and benzene ring for the systems **2a** and **2b**, respectively. These axes are close to the directions of reaction field from polar solvents induced by the electron transferred states. The π and π^* orbitals obtained by diagonalizing the dipole moments are considered to be stable to the electrostatic field from solvents.

3.2.3. σ Orbitals. We adopted the Boys' localized orbitals[43] (BLOs) to represent the σ orbitals from the following reasons. First, the BLOs are localized at the regions of chemical bonds and provide chemically intuitive description of electronic structures of molecules. The pathway analyses in terms of LMOs will give a graspable insight to the mechanism of intramolecular electron transfer. Second, the magnitude of interaction between BLOs is expected to be small enough to achieve a rapid convergence for the perturbation series, eq 9, as contrasted to the interactions between the localized atomic orbitals. This would be helpful to find out the dominant electron transfer paths. Finally, the BLOs are stable against the electrostatic field from solvents as shown in Appendix. As is well-known, electron transfer reactions are controlled by the solvent polarization and thus the BLOs seems to be suitable to describe the electronic structures of electron transfer systems in polar solvents.

For **1** and **2**, 138 and 141 occupied BLOs were obtained by applying the Boys' procedure to the occupied orbital space after excluding the π orbitals determined above. Each occupied BLO was well characterized to the core, nonbonding, and bonding orbitals of donor, acceptor, and spacer parts.

Since we used the split valence 3-21G basis set, the number of virtual orbitals is larger than that of valence antibonding orbitals in the present case. We therefore defined the valence antibonding orbital spaces with the use of natural localized antibonding orbitals[44] (NLABOs) obtained by diagonalizing the density matrices where the occupation numbers of the π orbitals of porphyrin, benzoquinone, and spacer benzene parts were set equal to zero. The COTs of σ^* unoccupied orbital set to the valence anti-bonding NLABOs were carried out to derive the valence antibonding orbital spaces. The BLO transformation in these orbital spaces finally gave 86 and 88 valence σ^* localized orbitals for **1** and **2**, respectively. The orbital set obtained thus is denoted to be the Basis 1.

There remains the outer set of orbitals in the virtual orbital space after defining the Basis 1. Unfortunately, there are nonnegligible interaction between the valence and outer orbitals and the importance of such interaction in evaluating the ECEs was pointed out by Liang et al.[24] in their study based on the natural bond orbitals.[44] It is expected that the valence−outer interaction is also important in the present model based on NLABO considering that the NLABOs used to define the valence space in Basis 1 are determined by the transformation within the space of natural bonding and antibonding orbitals. We therefore attempted to include the effect of valence−outer orbital interaction in defining new valence orbital sets. We constructed the Fock matrices in terms of the valence unoccupied and outer orbitals, and we diagonalized the reduced Fock matrices including one valence unoccupied orbital (i.e., π^* or σ^* localized orbital) and all the outer orbitals. Each of the diagonalization provides the modified valence orbital which is given as the eigen vector corresponding to the lowest eigen value. Since the modified valence unoccupied orbitals obtained after the sequence of diagonalizations are not orthogonal to one another, we further applied the symmetric orthogonalization to them. The resultant orbital set is referred to the Basis 2.

The σ^* orbitals of the porphyrin skeletons were excluded from the Basis 1 and 2 orbital sets in constructing the SECI wave functions because the electronic configurations representing the

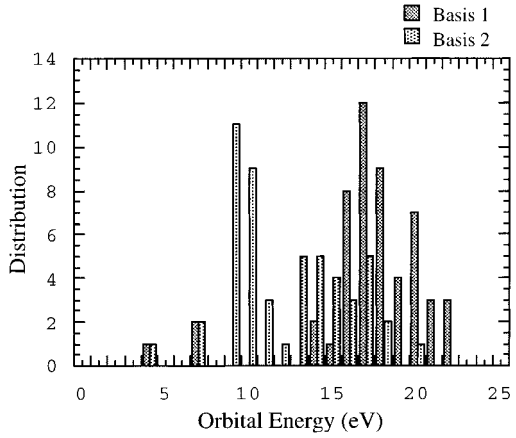

Figure 3. A histogram of orbital energies of the Basis 1 and Basis 2 sets for **1**.

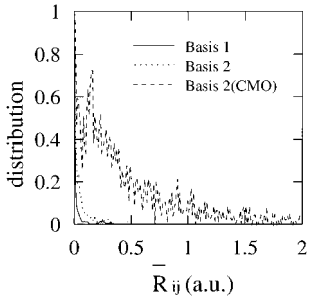

Figure 4. Distributions of absolute values of the transition dipole moments $\bar{R}_{ij}$ for **2a** with the Basis 1, 2, and 2(CMO) sets.

excitation to these σ^* orbitals are considered not to be important in the reaction process. The numbers of the spacer unoccupied orbitals thus became 50 and 52 for the system **1** and **2**, respectively.

3.2.4. Comparison of Basis 1 and 2. In Figure 3, a histogram of the energies of valence unoccupied orbitals both for Basis 1 and 2 sets for **2a** is presented. In the Basis 1, roughly speaking, there are two peaks at the regions of 4−7 eV and 14−22 eV. The lower and higher energy peaks consist of the π^* and σ^* orbitals, respectively. For the Basis 2, new two peaks appeared at the regions centered at 10 and 13 eV and these orbitals were identified as the σ^* orbitals of the C−H antibonding and C−C antibonding characters. Note that the σ^* skeletons of benzene and benzoquinone parts were still high in energy.

It is preferable to employ highly localized orbitals in order to distinguish the electron transfer pathways clearly. We evaluated the transition dipole moments between the orbitals to assess the degree of localization of the orbital sets derived here. As shown in Appendix, highly localized orbitals in the sense of the Boys's localization have small transition dipole moments. Figure 4 shows the distributions of absolute values of the transition dipole moments $\bar{R}_{ij}$,

$$\bar{R}_{ij} = \sqrt{\langle i|x|j\rangle^2 + \langle i|y|j\rangle^2 + \langle i|z|j\rangle^2} \tag{14}$$

calculated for the **2a** molecule with the use of Basis 1, Basis 2, and Basis 2(CMO). The Basis 2(CMO) orbitals were obtained by diagonalizing the Fock matrix defined in terms of Basis 2, and are therefore regarded as the canonical orbital set in the valence space. Because the Basis 1 was determined by the Boys's localization, the transition dipole moments have smaller values. On the other hand, there are large transition dipole moments in the case of Basis 2 (CMO). In general, such canonical orbitals are delocalized. The transition dipole moments for the Basis 2 are slightly larger than those for the Basis 1 because the Basis 2 orbitals were obtained by mixing the outer orbital components into the Basis 1 sets. Nevertheless, the Basis 2 seems to be acceptably localized compared to the Basis 2 (CMO).

3.3. Electronic States. The SECI wave functions for the reactant, product, and intermediate states were constructed with the donor, acceptor, and spacer orbitals determined above. The reactant electronic wave functions were given by diagonalizing the Hamiltonian matrix spanned by the configurations which correspond to single electron excitations from the π orbitals to the π^* orbitals of porphyrin. The lowest energy states were defined as the reactant state, Por*−Qui. The electronic states of the product defined by eq 12 contain cation states of porphyrin which have A_u- or B_{1u}-like symmetries. Unfortunately, it is not possible to determine the relative stability of these cation states at the present level of the calculations.[45] We therefore investigated the ECE and the pathways for each case where the product and intermediate electronic states include each of cation states of porphyrin. Diagonalizing the Hamiltonian matrix spanned by the configurations which have the excitations from each of the π orbitals of porphyrin to the valence π^* orbitals of quinone, the lowest energy state was defined as the product state for each of the cation states, $Por^+(A_u) - Qui^-$ and $Por^+(Blu) - Qui^-$.

4. Results and Discussion

4.1. Electron Transfer vs Hole Transfer. Taking into account the intermediate states given in eq 13, we can define three different types of pathways as discussed by Liang et al.,[25] which are schematically illustrated in Figure 5. One is the pure "electron" transfer (e-transfer) involving only the intermediate states $|\phi_{I_i[d\to s^*]}\rangle$ as shown in Figure 5a. The contribution from e-transfer pathways, $V_{RP}^{\mathrm{indir(e)}}$ is given by

$$V_{RP}^{\mathrm{indir(e)}} = \sum_{i,j} V_{R\,I_i[d\to s^*]} G_{ij}^{\mathrm{e}} V_{I_j[d\to s^*]P} \tag{15}$$

where G_{ij}^{e} is the matrix elements of the Green function of e-transfer:

$$\hat{G}^{\mathrm{e}} = \frac{1}{E - \hat{H}_{\mathrm{el}}^{I[d\to s^*]}} \tag{16}$$

The other pathways, ex/h- and h/ex-transfers in Figure 5b and c, are regarded as the "hole" transfer (h-transfer) types accompanied by the excitation transfers from porphyrin to quinone. The ex/h-type is represented by the excitation transfer followed by the h-transfer and the h/ex-type is the reverse. These are expressed by the intermediate states $|\phi_{I_i[s\to a^*]}\rangle$ and $|\phi_{I_i[s\to d^*]}\rangle$, and the contributions from these pathways, $V_{RP}^{\mathrm{indir(ex/h)}}$ and $V_{RP}^{\mathrm{indir(h/ex)}}$, are calculated by the analogous formulas to eq 15 and 16.

We calculated $V_{RP}^{\mathrm{indir(e)}}$, $V_{RP}^{\mathrm{indir(ex/h)}}$ and $V_{RP}^{\mathrm{indir(h/ex)}}$ for the system **1** with the Basis 2 spacer orbitals. For computational simplicity, we employed only Goutermans 4 orbitals[42] (i.e., the $2a_u$ and $5b_{1u}$ π orbitals and $4b_{3g}$ and $4b_{2g}$ π^* ones for porphyrin and the lowest unoccupied π^* orbital for quinone, respectively). The tunneling energies E in eq 4 were set to be the energies of the product states.

In Table 3, the calculated $V_{RP}^{\mathrm{indir(e)}}$, $V_{RP}^{\mathrm{indir(ex/h)}}$, and $V_{RP}^{\mathrm{indir(h/ex)}}$ are tabulated. $V_{RP}^{\mathrm{indir(ex/h)}}$ and $V_{RP}^{\mathrm{indir(h/ex)}}$ are significantly smaller than $V_{RP}^{\mathrm{indir(e)}}$, indicating that the pathways involving the h-

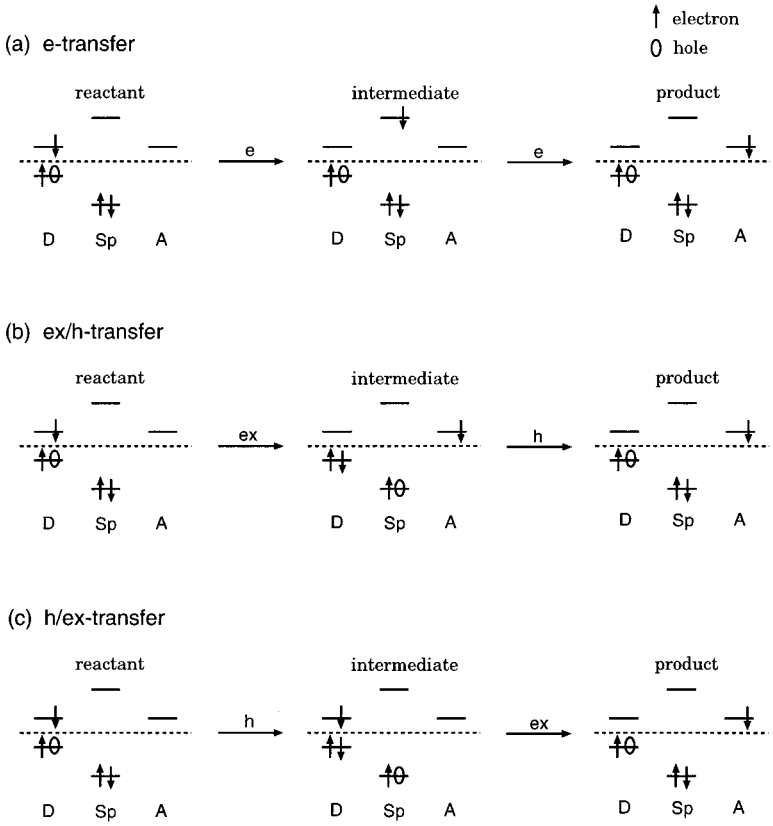

Figure 5. Schematic depiction of (a) e-transfer, (b) ex/h-transfer and (c) h/ex-transfer.

TABLE 3: Electronic Coupling Elements of e-, ex/h-, and h/ex-transfers (cm^{-1}) for 1

	A_u	B_{1u}
$V_{RP}^{\text{indir(e)}}$	4.24	6.28
$V_{RP}^{\text{indir(ex/h)}}$	-5.73×10^{-2}	-2.10×10^{-3}
$V_{RP}^{\text{indir(h/ex)}}$	-6.32×10^{-3}	5.28×10^{-4}

TABLE 4: Excitation Energy (eV) of Reactant and Product States

	1	**2a**	**2b**
Por*−Qui	3.059	3.059	3.059
$Por^+(A_u)-Qui^-$	5.634	5.611	5.422
$Por^+(B_{1u})-Qui^-$	6.098	6.076	5.887

transfers play a minor role in determining the ECEs. This comes from small electronic interaction elements $V_{R\,I_i[s\rightarrow a^*]}$ and $V_{I_i[s\rightarrow d^*]P}$ in $V_{RP}^{\text{indir(ex/h)}}$ and $V_{RP}^{\text{indir(h/ex)}}$, respectively, which include only two electron integrals of the SECI matrix elements, eq 10. It is noted that the hybrid "electron/hole" type pathways represented by the configurations in eq 13d are expected to give minor contributions because the electronic coupling elements are constituted by only two electron integrals. Since the e-transfer couplings $V_{RP}^{\text{indir(e)}}$ are the dominant contributions in the indirect electronic couplings for the present charge separation processes, we consider only the e-transfer couplings and neglect the contributions involving the h-transfers in the following analyses.

4.2. Overall Electronic Coupling Element. The overall electronic coupling elements V_{RP} were calculated with the SECI matrix elements of intermediate states using the Basis 1 and 2 spacer orbitals. In constructing the reactant and product states, we adopted all the the valence donor and acceptor π^* orbitals, 11 and 4 π^* orbitals of porphyrin and quinone, respectively. The excitation energies of the reactant and product states are presented in Table 4. The calculated excitation energies are overestimated by about 1 eV. As is easily seen, the reactant states have almost the same excitation energies for all the molecules. On the other hand, the energy of the product state for **2b** is significantly lower than the energies for **1** and **2a**. This stabilization of the product state for **2b** comes from a stronger electrostatic interaction between the donor and acceptor parts due to the shorter donor−acceptor distance.

The resultant ECEs are summarized in Table 5. In the A_u case, the ECEs with Basis 1 and 2 were evaluated to be 6.27 and 6.75 cm^{-1} for **1**. These ECEs are slightly smaller than those for **2a**, 8.55 and 8.81 cm^{-1}, respectively. The relative position of the donor and acceptor parts in **2a** is similar to that in **1**, although **2a** involves the bicyclo ring in the spacer part. It therefore seems that the presence of the bicyclo ring does not cause a large difference in the magnitude of ECE. On the other hand, the ECEs for **2b**, 18.86 and 27.29 cm^{-1} by Basis 1 and 2, respectively, are much larger than those for **1** and **2a**. Accordingly, the difference in geometry between **2a** and **2b** produce a large difference in the ECEs. It is noted that the ECE of **2b** calculated with Basis 2 is significantly larger than that with Basis 1, though both the basis sets provide similar values of the ECE for **1** and **2a**.

For the B_{1u} states, the ECEs for **1**, **2a**, and **2b** were calculated to be 4.64, 6.45, and 10.24 cm^{-1} with Basis 1, respectively. The relative magnitudes of these ECEs are in qualitative agreement with those in the A_{1u} case. In contrast to the other cases, the ECE for **2b** is reduced to 7.38 cm^{-1} using the Basis 2. We will discuss this point later.

Considering the experimental result[38] that the molecule **2** shows much faster electron transfer rate than **1**, it is likely that the A_u type state for **2b** is responsible to the actual electron transfer process. This is consistent with the ordering of product

TABLE 5: Overall Electronic Coupling Elements V_{RP} (cm^{-1})

	A_u		B_{1u}	
V_{RP}	Basis 1	Basis 2	Basis 1	Basis 2
1	6.27	6.57	4.64	8.38
2a	8.55	8.81	6.45	8.88
2b	18.86	27.29	10.24	7.38

state energies in Table 4, where the energy of the A_u type product state for **2b** is the lowest.

4.3. Decomposition of Overall Electronic Coupling Elements. As shown above, the overall ECEs depend on the characters of spacers and the electronic structures of the intermediate and product states. The pathway analyses would provide a clear explanation of the origin of these dependences by finding out the dominant pathways to determine the ECEs. However, a large number of pathways, the terms of the expansion in eq 9, are generated because of large intermediate space in the present case, which make the pathway analyses complicated. We therefore divided the intermediate space into several subspaces and decomposed the overall ECE into the contributions from the intermediate subspaces based on eqs 2 and 7. One of the contributions is the direct ECE, eq 3. For the indirect ECE, we classified the intermediate states eq 13a into three types. One is the configuration where the π^* orbital of benzene part (π^*(Ben)) is occupied by an electron because the character of benzene π^* orbitals is obviously different from that of the σ^* orbitals. The states where the σ^* orbital are involved were further divided into two types: one is the configurations involving the σ^* orbitals in the two methyl groups attached to porphyrin (σ^*(DMe)) and another is the remaining σ^* orbital states (σ^*). In eq 7, the unperturbed Green function $\hat{G}^0(E)$ is expressed by the sum of the Green functions for the intermediate subspaces, i.e.

$$\hat{G}^0(E) = \sum_A \hat{G}^0_A(E) \tag{17}$$

where $\hat{G}^0_A(E)$ is the Green function for the subspace A. It is noted that $\hat{G}^0(E)$ is defined using the block diagonal Hamiltonian matrix and the perturbation part $\hat{V}$ in eq 7 corresponds to the block off-diagonal Hamiltonian matrix. The indirect ECE is thus given as the sum of contributions from three terms, $V^{\mathrm{indir}}_{RP}[A]$, $V^{\mathrm{indir}}_{RP}[A, B]$, and $V^{\mathrm{indir}}_{RP}[A, B, C]$.

$V^{\mathrm{indir}}_{RP}[A]$, the contributions from the pathways involving only the subspace A, is given by

$$V^{\mathrm{indir}}_{RP}[A] = \langle \phi_R \hat{V} \hat{G}^0_A(E) \hat{V} | \phi_P \rangle \tag{18}$$

The terms which include both $\hat{G}^0_A(E)$ and $\hat{G}^0_B(E)$ in eq 7 constitute $V^{\mathrm{indir}}_{RP}[A, B]$. This contribution was estimated with the relation,

$$V^{\mathrm{indir}}_{RP}[A, B] = \langle \phi_R | \hat{V} \hat{G}^0_{A\oplus B}(E) \hat{V} | \phi_P \rangle - V^{\mathrm{indir}}_{RP}[A] - V^{\mathrm{indir}}_{RP}[B] \tag{19}$$

where $\hat{G}^0_{A\oplus B}(E)$ is the Green function of the Hamiltonian defined in terms of the subspaces A and B. The third contribution $V^{\mathrm{indir}}_{RP}[A, B, C]$ is given by the analogous relation to $V^{\mathrm{indir}}_{RP}[A, B]$, i.e.

$$V^{\mathrm{indir}}_{RP}[A, B, C] = V^{\mathrm{indir}}_{RP} - \sum_X V^{\mathrm{indir}}_{RP}[X] - \sum_{X>Y} V^{\mathrm{indir}}_{RP}[X,Y] \tag{20}$$

TABLE 6: Decomposed Electronic Coupling Elements (cm^{-1}) for 1

	A_u		B_{1u}	
	Basis 1	Basis 2	Basis 1	Basis 2
V^{dir}_{RP}	1.14		0.96	
V^{indir}_{RP}	5.13	5.43	3.68	7.42
$V^{\mathrm{indir}}_{RP}[\sigma^*(\mathrm{DMe})]$	−0.03	−0.05	0.01	0.06
$V^{\mathrm{indir}}_{RP}[\pi^*(\mathrm{Ben})]$	3.30	3.62	4.04	4.36
$V^{\mathrm{indir}}_{RP}[\sigma^*]$	1.39	0.02	−1.20	−0.62
$V^{\mathrm{indir}}_{RP}[\sigma^*(\mathrm{DMe}), \pi^*(\mathrm{Ben})]$	−0.15	−0.14	0.04	0.11
$V^{\mathrm{indir}}_{RP}[\sigma^*(\mathrm{DMe}), \pi^*]$	−0.03	−0.24	0.02	0.23
$V^{\mathrm{indir}}_{RP}[\pi^*(\mathrm{Ben}), \sigma^*]$	0.69	2.44	0.75	3.08
$V^{\mathrm{indir}}_{RP}[\sigma^*(\mathrm{DMe}), \pi^*(\mathrm{Ben}), \sigma^*]$	0.04	−0.22	0.02	0.20

TABLE 7: Decomposed Electronic Coupling Elements (cm^{-1}) for 2a

	A_u		B_{1u}	
	Basis 1	Basis 2	Basis 1	Basis 2
V^{dir}_{RP}	2.28		0.47	
V^{indir}_{RP}	6.27	6.53	5.98	8.41
$V^{\mathrm{indir}}_{RP}[\sigma^*(\mathrm{DMe})]$	−0.06	−0.05	0.04	0.08
$V^{\mathrm{indir}}_{RP}[\pi^*(\mathrm{Ben})]$	4.28	4.57	4.75	4.93
$V^{\mathrm{indir}}_{RP}[\sigma^*]$	0.63	−0.18	−0.82	−0.51
$V^{\mathrm{indir}}_{RP}[\sigma^*(\mathrm{DMe}), \pi^*(\mathrm{Ben})]$	−0.14	−0.13	0.01	0.79
$V^{\mathrm{indir}}_{RP}[\sigma^*(\mathrm{DMe}), \sigma^*]$	0.00	−0.18	0.00	0.21
$V^{\mathrm{indir}}_{RP}[\pi^*(\mathrm{Ben}), \sigma^*]$	1.64	2.67	1.97	3.44
$V^{\mathrm{indir}}_{RP}[\sigma^*(\mathrm{DMe}), \pi^*(\mathrm{Ben}), \sigma^*]$	−0.08	−0.17	0.03	−0.53

TABLE 8: Decomposed Electronic Coupling Elements (cm^{-1}) for 2b

	A_u		B_{1u}	
	Basis 1	Basis 2	Basis 1	Basis 2
V^{dir}_{RP}	9.62		−0.61	
V^{indir}_{RP}	9.24	17.67	10.85	7.99
$V^{\mathrm{indir}}_{RP}[\sigma^*(\mathrm{DMe})]$	1.05	0.52	−0.77	−0.50
$V^{\mathrm{indir}}_{RP}[\pi^*(\mathrm{Ben})]$	6.25	6.25	7.89	7.81
$V^{\mathrm{indir}}_{RP}[\sigma^*]$	−0.62	1.32	0.75	0.46
$V^{\mathrm{indir}}_{RP}[\sigma^*(\mathrm{DMe}), \pi^*(\mathrm{Ben})]$	−0.39	−0.34	0.00	0.25
$V^{\mathrm{indir}}_{RP}[\sigma^*(\mathrm{DMe}), \sigma^*]$	0.57	5.73	−0.38	−4.88
$V^{\mathrm{indir}}_{RP}[(\pi^*(\mathrm{Ben}), \sigma^*]$	2.54	4.59	3.38	5.40
$V^{\mathrm{indir}}_{RP}[\sigma^*(\mathrm{DMe}), \pi^*(\mathrm{Ben}), \sigma^*]$	−0.16	−0.40	−0.02	−0.55

The results of decomposition analyses of the ECEs are summarized in Tables 6−8. The differences of the ECE valuesbetween the two basis sets as discussed above are clearly understood by the decomposition analyses. For all the cases, $V^{\mathrm{indir}}_{RP}[\pi^*(\mathrm{Ben}), \sigma^*]$ with Basis 2 are larger than those with Basis 1. For the **2b** system, Basis 2 yields larger magnitudes of $V^{\mathrm{indir}}_{RP}[\sigma^*(\mathrm{DMe}), \sigma^*]$ compared to Basis 1, though the signs are different between the A_u and B_{1u} symmetries. These come from the diffuseness of σ^* orbitals in Basis 2 which are improved by including the outer orbitals. The difference in the signs of $V^{\mathrm{indir}}_{RP}[\sigma^*(\mathrm{DMe}), \sigma^*]$ is attributed to the interaction mode of the dimethyl σ^* orbitals with the porphyrin π^* ones.

The contributions from indirect ECEs V^{indir}_{RP} are dominant in all systems except for **2b** in the A_u case. The direct contribution is $\sim 1/3$ of V_{RP} in **2b** with Basis 2, 9.26 cm^{-1}, while these

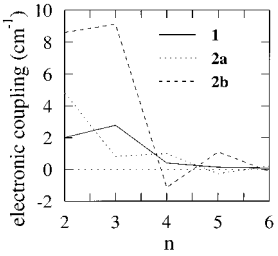

Figure 6. Contributions of the *n*th order terms of eq 9 in the Basis 2 case.

terms in the other cases are 1−2 cm^{-1}. As seen in the tables, $V_{RP}^{\text{indir}}[\pi^*(\text{Ben})]$ are the main contributions to V_{RP}^{indir} and much larger than $V_{RP}^{\text{indir}}[\sigma^*]$, indicating that the spacer π^* orbitals provide important routes for electron transfer in the present systems. Note that the previous studies mainly focused on the $V_{PR}^{\text{indir}}[\sigma^*]$ term in hydrocarbon spacers. The second important terms are $V_{PR}^{\text{indir}}[\pi^*(\text{Ben}), \sigma^*]$ for all the system. Compared to the other systems, the magnitudes of $V_{RP}^{\text{indir}}[\sigma^*(\text{DMe}), \sigma^*]$ is notable in **2b** and the total V_{RP} is enhanced by this term in the A_u case while it is reduced in the B_{1u} case.

4.4. Pathway Analysis. In order to obtain more detail information on the mechanism of intramolecular electron transfer process, we carried out the pathway analyses based on the perturbation series given in eq 9. Since the intermediate states both in the A_u and B_{1u} cases have the similar structure of Hamiltonian matrix and the difference of ECEs between the two cases are mainly determined by the matrix elements between the reactant and intermediate states, the pathway analyses were performed only for the case of A_u. The important pathways of the B_{1u} case would be deduced from the results of analyses for the A_u.

Before proceeding the pathway analyses, the convergence of the perturbation series in eq 9 was examined. Figure 6 shows the contributions from the *n*th order terms to the ECEs in the Basis 2 cases, where $n - 1$ is the number of the intermediate states involved. It is found that the ECE values obtained by the perturbation calculations up to the sixth order well reproduce the overall ECEs and the errors were within 1%. As is seen in Figure 6, the contributions from the second and third terms are large. It is noted that the nearest-neighbor pathways as in the McConnell Model,[46] which are mainly expressed by the fifth or sixth terms, seem to give minor contributions in the present case.

We focused on the third order pathways where the electron propagates through two intermediate states strongly coupled to the reactant and product states, respectively. We defined 18 intermediate states denoted by the states I−III and 1−15. In the states I and II, the π^* and σ^* orbitals of benzene part as in Figure 7 are occupied, respectively. The state III corresponds to the intermediate states involving the C−H σ^* orbital in the methyl group linked to porphyrin. The states 1−15 are described by the excitation to the spacer C−C and C−H σ^* orbitals denoted by the numbers in the figure. The pathways through the states I, II, and III are correlated to the decomposed ECEs, $V_{RP}^{\text{indir}}[\pi^*(\text{Ben}), \sigma^*]$, $V_{RP}^{\text{indir}}[\sigma^*]$ and $V_{RP}^{\text{indir}}[\sigma^*(\text{DMe}), \sigma^*]$, respectively.

Figures 8−10 show the contributions from the third-order pathways calculated with Basis 2. For **1** and **2a**, the contributions from the pathways through II which mainly contribute to $V_{RP}^{\text{indir}}[\sigma^*]$ are found to have relatively large absolute values. They exhibit, however, the destructive interference with one another because they do not have the same sign. As contrasted

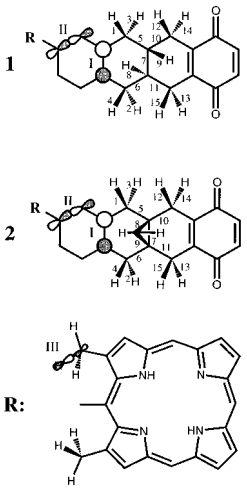

Figure 7. Definition of symbol for the intermediate states.

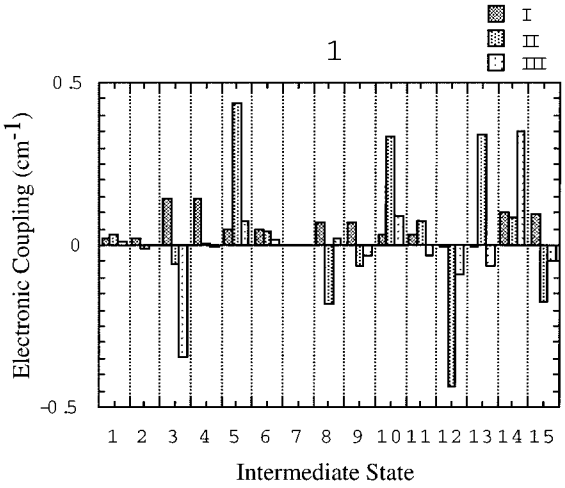

Figure 8. Contribution of the third order terms to the ECEs for **1** in the Basis 2 case.

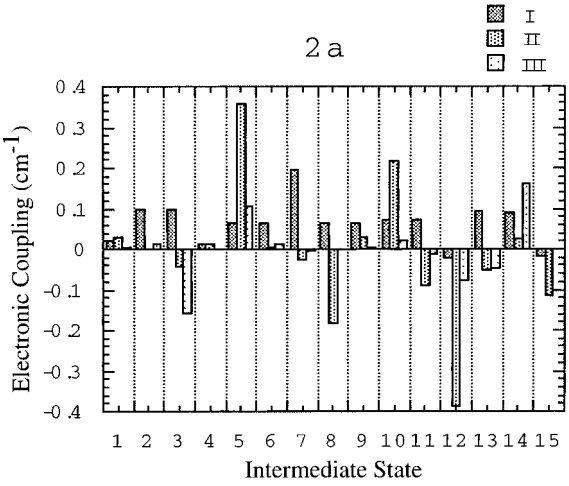

Figure 9. Contribution of the third order terms to the ECEs for **2a** in the Basis 2 case.

with the state II case, the dominant contributions from the state I, which are responsible to $V_{RP}^{\text{indir}}[\pi^*(\text{Ben}), \sigma^*]$, have the same sign, implying that these give constructive interference, although the contributions are relatively small. Thus there are different features of the interferences between the states I and II and these interferences enhance $V_{RP}^{\text{indir}}[\pi^*(\text{Ben}), \sigma^*]$ and

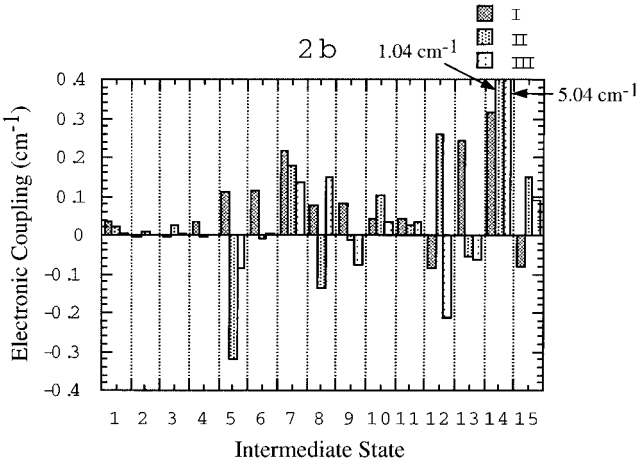

Figure 10. Contribution of the third order terms to the ECEs for **2b** in the Basis 2 case.

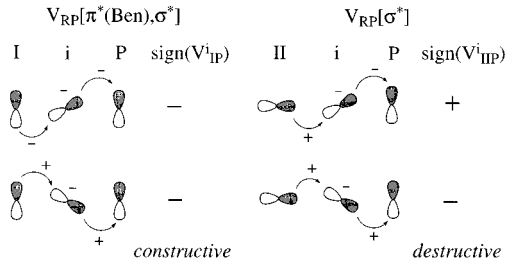

Figure 11. A diagram of orbitals for pathways contributing $V_{RP}[\pi^*(\text{Ben}),\sigma^*]$ and $V_{RP}[\sigma^*]$.

reduce $V_{RP}^{\text{indir}}[\sigma^*]$ as appeared in Tables 6−8. In order to understand the origin of the difference in the interference mentioned, we consider the orbital diagram in Figure 11. The electronic interaction between the states *i* and *j* through the state *k*, V_{ij}^k, is expressed by

$$V_{ij}^k = V_{ik}\frac{1}{E - E_k}V_{kj} \tag{21}$$

In the present case, the energy denominator is negative. As well-known, the direct electronic interaction between the states *i* and *k*, V_{ik}, has opposite sign to the overlap integral of these states S_{ik}. Consequently, the sign of V_{ij}^k is given by

$$\text{sign}(V_{ij}^k) = -\text{sign}(S_{ik})\text{sign}(S_{kj}) \tag{22}$$

The orbitals occupied in the state I are in parallel to the product orbital while those in II are perpendicular. As shown in Figure 11, the indirect interaction between the state I and the product state through the intermediate states undergoes constructive interference between the pathways involved. On the other hand, destructive interference is given for the indirect interaction between the state II and the product.

It is noted that the contributions from the pathways through the intermediate state 7 is very small in the system **1**. Since the subsystem **1′** has C_2 symmetry, the spacer and acceptor orbitals are well characterized by the C_2 point group. The σ^* orbital at the site 7 in Figure 7 has a very small overlap with the acceptor orbital because these orbitals belong to the *b* and *a* irreducible representation in **1′**, respectively. On the other hand, the intermediate states 7 for **2a** and **2b** contribute significantly. This is because the subsystems **2a′** and **2b′** have C_s symmetry and both the intermediate states 7 and the product one belong to the same irreducible representation, A″, which gives a strong interaction between these two states. The contributions from the C−H antibonding orbitals in the bicyclo ring for **2** were found to be almost zero. This also comes from the symmetry relation between the C−H antibonding and acceptor orbitals.

For **2b**, the intermediate state 14 strongly interacts with the state II and III, which results from short distance and matched mutual orientation between the σ^* bonds characterizing those intermediate states due to the bended geometry of the spacer part.

5. Conclusion

The ECEs were investigated for the long-range electron transfer reactions in the compounds **1** and **2** which comprise porphyrin and benzoquinone as electron donor and acceptor, respectively, linked by organic spacers. We calculated the ECEs by ab initio MO calculations. The reactant, product and intermediate states were determined by the SECI wave functions composed of the localized donor, acceptor, and spacer orbitals. The ECE was defined by the sum of the direct or through space term V_{RP}^{dir} and the indirect or through bond one V_{RP}^{indir}, and these terms were evaluated with the SECI matrix elements. In order to elucidate the character of the ECE, the decomposition and pathway analyses were carried out.

We compared the magnitudes of ECEs coming from the "electron" and "hole" transfer mechanisms. The "electron" transfer mechanism was found to dominantly contribute to the present photoinduced electron transfer reactions. It was shown by the geometry optimizations for the subsystems that the compound **2** has two stable structures, **2a** and **2b**, whose energies are almost the same. The ECE of **2b** was evaluated to be larger than those of **1** and **2a**. It means that the ECEs depend strongly on the geometries. It is noted that the relative magnitude of the ECEs of **1** and **2b** is consistent with experimental findings.[38] The decomposition analyses revealed that the indirect ECEs are significant and the π^* orbitals of benzene in the spacers play an important role in determining the magnitudes of the indirect ECEs. It was also found that the σ^* states of the dimethyl groups also give large contributions to the indirect ECEs for **2b**. These results were obtained by the pathway analyses and the significance of the interference between different pathways was demonstrated.

We employed the SECI wave functions in describing the reactant, product, and intermediate states. Although the electron correlation effect may be important to reproduce the excitation energies of porphyrin, it is computationally prohibited to include doubly and triply excited configurations for large systems as the present case. In spite of a crude approximation for the wave functions, the present treatment is expected to provide a reasonable description for the electronic structure of electron transfer system because the predominant configurations for the electronic structures of Q-bands of porphyrin excited states are the singly excited configurations in the Gouterman's four orbital space.[47]

It is noted that these electron transfer reactions take place only in polar solvents. In a future study, we will investigate the role of polar solvent on the reaction mechanism with molecular dynamics calculations. It was shown that the electronic wave functions determined in the present study are stable against the electronic static field from polar solvent. Using the molecular models constructed in the present study is expected to give a clear description of the reaction mechanism.

Acknowledgment. The authors are grateful to Professor Y. Sakata, T. Okada, and Mr. K. Araki for their valuable comments

and discussions. Numerical calculations were carried out at IMS Computer Center. This work was supported by the Grants in Aid for Scientific Research from the Ministry of Education. S.H. acknowledges the Research Fellowships of the Japan Society for the Promotion of Science for Young Scientists for support of this research.

Appendix

For the classical solvent model, the electrostatic solvation energy is expressed using the one electron operator,

$$\hat{H}_{\mathrm{solv}} = \sum_{\alpha,i} \frac{q_\alpha^{\mathrm{solv}}}{r_{\alpha i}} \tag{23}$$

where q_α^{solv} is the point charge on the interaction site α of the solvent and $r_{\alpha i}$ is the distance between α and the electron i. In the present case, the SECI wave functions which are stable to the electrostatic field are defined by the unitary transformation which reduces the off-diagonal elements of the solvation energy operator

$$H_{rs}^{\mathrm{solv}} = \langle \Phi^1(a \rightarrow r) | \hat{H}_{\mathrm{solv}} | \Phi^1(a \rightarrow s) \rangle = \left\langle r \left| \sum_\alpha \frac{q_\alpha^{\mathrm{solv}}}{r_\alpha} \right| s \right\rangle \tag{24}$$

In the reaction dipole field approximation, the off-diagonal elements are approximated by

$$H_{rs}^{\mathrm{solv}} \simeq \langle r | \boldsymbol{r} | s \rangle \sum_\alpha \frac{\boldsymbol{R}_\alpha - \boldsymbol{r}_0}{|\boldsymbol{R}_\alpha - \boldsymbol{r}_0|^3} \tag{25}$$

where $\boldsymbol{r}$, $\boldsymbol{R}_\alpha$ and $\boldsymbol{r}_0$ are coordinates of the electron, the interaction site α and the center of mass of solute, respectively. Accordingly, the stable electronic states are expected to be given with the MOs whose off-diagonal matrix elements of the dipole moment operator have small absolute values.

The Boys' localized orbitals are determined by solving the stationary problem for the functional[43]

$$I_{\mathrm{Boys}} = \prod_{i>j} [|\langle i | \boldsymbol{r} | i \rangle - \langle j | \boldsymbol{r} | j \rangle|^2] \tag{26}$$

The second derivative matrix of I_{Boys} with respect to the variations of orbitals is negative-definite at the stationary point, that is, the Boys' localized orbitals give the maximum value for I_{Boys}. As is easily shown, the Boys' localized orbitals are also a stationary point for the value

$$I = \prod_{i>j} [|\langle i | \boldsymbol{r} | j \rangle|^2] \tag{27}$$

and the second derivative matrix of I at the stationary point is positive definite. Thus the Boys' localized orbitals give small absolute values of the off-diagonal matrix element of the dipole moment operator. The electronic states which are stable against the reaction electrostatic field of the solvent are therefore expected to be obtained with the Boys' localized orbitals according to eq 25.

References and Notes

(1) Wasielewski, M. R. *Chem. Rev.* **1992**, *92*, 435.
(2) Miller, J. R.; Beits, J. V.; Huddleston, R. K. *J. Am. Chem. Soc* **1984**, *106*, 5057.
(3) Closs, G. L.; Calcaterra, L. T.; Green, N. J.; Penfield, K. W.; Miller, J. R. *J. Phys. Chem.* **1986**, *90*, 3674.
(4) Closs, G. L.; Miller, J. R. *Science* **1988**, *240*, 440.
(5) Closs, G. L.; Piotrowiak, P.; MacInnis, J. M.; Fleming, G. R. *J. Am. Chem. Soc.* **1988**, *110*, 2652.
(6) Closs, G. L.; Johnson, M. D.; Miller, J. R.; Piotrowiak, P. *J. Am. Chem. Soc.* **1989**, *111*, 3751.
(7) Johnson, M. D.; Miller, J. R.; Green, N. S.; Closs, G. L. *J. Phys. Chem.* **1989**, *93*, 1173.
(8) Oliver, A. M.; Craig, D. C.; Paddon-Row, M. N.; Kroon, J.; Verhoeven, J. W. *Chem. Phys. Lett.* **1988**, *150*, 366.
(9) Smit, K. J.; Warman, J. M.; Haas, M. P. D.; Paddon-Row, M. N.; Oliver, A. M. *Chem. Phys. Lett.* **1988**, *152*, 177.
(10) Wasielewski, M. R.; Niemczyk, M. P. *J. Am. Chem. Soc.* **1984**, *106*, 5043.
(11) Sakata, Y.; Nakashima, S.; Goto, Y.; Tatemitsu, H.; Misumi, S.; Asahi, T.; Hagihara, M.; Nishikawa, S.; Okada, T.; Mataga, N. *J. Am. Chem. Soc.* **1989**, *111*, 8979.
(12) Hoffmann, R. *Acc. Chem. Res.* **1971,** *4*, 1.
(13) Paddon-Row, M. N. *Acc. Chem. Res.* **1982**, *15*, 245.
(14) Marcus, R. A.; Sutin, N. *Biochim. Biophys. Acta* **1985**, *811*, 265.
(15) Larsson, S. *J. Am. Chem. Soc.* **1981**, *103*, 4034.
(16) Ohta, K.; Closs, G. L.; Morokuma, K.; Green, N. J. *J. Am. Chem. Soc.* **1986**, *108*, 1319.
(17) Gruschus, J. M.; Kuki, A. *J. Phys. Chem.* **1993**, *97*, 5581.
(18) Stuchebrukhov, A. A.; Marcus, R. A. *J. Phys. Chem.* **1995**, *99*, 7581.
(19) Kurnikov, I. V.; Beratan, D. N. *J. Chem. Phys.* **1996**, *105*, 9561.
(20) Ratner, M. A. *J. Phys. Chem.* **1990,** *94*, 4877.
(21) Jordan, K. D.; Paddon-Row, M. N. *Chem. Rev.* **1992**, *92*, 395.
(22) Jordan, K. D.; Paddon-Row, M. N. *J. Phys. Chem.* **1992**, *96*, 1188.
(23) Newton, M. D. *Chem. Rev.* **1991,** *91*, 767.
(24) Liang, C.; Newton, M. D. *J. Phys. Chem.* **1992**, *96*, 2855.
(25) Liang, C.; Newton, M. D. *J. Phys. Chem.* **1993**, *97*, 3199.
(26) Naleway, C. A.; Curtiss, L. A.; Miller, J. R. *J. Phys. Chem.* **1991,** *95*, 8434.
(27) Curtiss, L. A.; Naleway, C. A.; Miller, J. R. *J. Phys. Chem.* **1995**, *99*, 1182.
(28) Koga, N.; Sameshima, K.; Morokuma, K. *J. Phys. Chem.* **1993**, *97*, 13117.
(29) Siddarth, P.; Marcus, R. A. *J. Phys. Chem.* **1993**, *97*, 2400.
(30) Siddarth, P.; Marcus, R. A. *J. Phys. Chem.* **1993**, *97*, 13078.
(31) Stuchebrukhov, A. A. *J. Chem. Phys.* **1996**, *104*, 8424.
(32) Onuchic, J. N.; Beratan, D. N. *J. Chem. Phys.* **1990,** *92*, 722.
(33) Beratan, D. N.; Onuchic, J. E.; Bowler, J. N. B. B. E.; Gray, H. B. *J. Am. Chem. Soc.* **1990**, *112*, 7915.
(34) Beratan, D. N.; Betts, J. N.; Onuchic, J. N. *Science* **1991**, *252*, 1285.
(35) Betts, J. N.; Beratan, D. N.; Onuchic, J. E. *J. Am. Chem. Soc.* **1992**, *114*, 4043.
(36) Beratan, D. N.; Betts, J. N.; Onuchic, J. E. *J. Phys. Chem.* **1992**, *96*, 2852.
(37) Regan, J. J.; Risser, S. M.; Beratan, D. N.; Onuchic, J. N. *J. Phys. Chem.* **1993**, *97*, 13083.
(38) Sakata, Y.; Araki, K.; Okada, T. Private communication.
(39) Foresman, J. B.; Head-Gordon, M.; Pople, J. A.; Frisch, M. J. *J. Phys. Chem.* **1992**, *96*, 135.
(40) Löwdin, P. O. *J. Chem. Phys.* **1951**, *19*, 1396.
(41) King, H. F.; Stanton, R. E.; Kim, H.; Wyatt, R. E.; Parr, R. G. *J. Chem. Phys.* **1967**, *47*, 1936.
(42) Gouterman, M. *J. Chem. Phys.* **1959**, *30*, 1139.
(43) Foster, J. M.; Boys, S. F. *Rev. Mod. Phys.* **1960**, *32*, 300.
(44) Reed, A. E.; Curtiss, L. A.; Weinhold, F. *Chem. Rev.* **1988**, *88*, 899.
(45) Ghosh, A.; Almlof, J. *Chem. Phys. Lett.* **1993**, *213*, 519.
(46) McConnell, H. M. *J. Chem. Phys.* **1961**, *35*, 508.
(47) Masthay, M. B.; Findsen, L. A.; Pierce, B. M.; Bocian, D. F.; Lindsey, J. S.; Birge, R. R. *J. Chem. Phys.* **1986**, *84*, 3901.